Crystal structure of *Pseudomonas aeruginosa* RsaL bound to promoter DNA reaffirms its role as a global regulator involved in quorum-sensing

Huaping Kang[1],[†], Jianhua Gan[2],[†], Jingru Zhao[1],[†], Weina Kong[1], Jing Zhang[2], Miao zhu[1], Fan Li[1], Yaqin Song[1], Jin Qin[1] and Haihua Liang[1],[*]

[1]Key Laboratory of Resources Biology and Biotechnology in Western China, Ministry of Education, College of Life Science, Northwest University, Xi'an, Shaanxi 710069, China and [2]Department of Physiology and Biophysics, School of Life Sciences, Fudan University, Shanghai 200438, China

ABSTRACT

***Pseudomonas aeruginosa* possesses at least three well-defined quorum-sensing (QS) (*las*, *rhl* and *pqs*) systems that control a variety of important functions including virulence. RsaL is a QS repressor that reduces QS signal production and ensures homeostasis by functioning in opposition to LasR. However, its regulatory role in signal homeostasis remains elusive. Here, we conducted a ChIP-seq assay and revealed that RsaL bound to two new targets, the intergenic regions of PA2228/PA2229 and *pqsH/cdpR*, which are required for PQS synthesis. Deletion of *rsaL* reduced transcription of *pqsH* and *cdpR*, thus decreasing PQS signal production. The Δ*rsaL* strain exhibited increased pyocyanin production and reduced biofilm formation, which are dependent on CdpR or PqsH activity. In addition, we solved the structure of the RsaL–DNA complex at a 2.4 Å resolution. Although the overall sequence similarity is quite low, RsaL folds into a HTH-like structure, which is conserved among many transcriptional regulators. Complementation results of the *rsaL* knockout cells with different *rsaL* mutants further confirmed the critical role of the DNA-binding residues (including Arg20, Gln27, Gln38, Gly35, Ser37 and Ser42) that are essential for DNA binding. Our findings reveal new targets of RsaL and provide insight into the detailed characterization of the RsaL–DNA interaction.**

INTRODUCTION

Bacteria use small diffusible molecules, also known as autoinducers, as signals for monitoring population density and coordinating gene regulation via a process termed quorum-sensing (QS) (1,2). Many Gram-negative bacterial species, including several human and plant pathogens, use acylated homoserine lactones (AHLs) as QS signal molecules (3,4). AHLs are synthesized by LuxI-type synthases and detected by LuxR-type regulators, which serve as the signal receptors. Once AHL concentration reaches a specific threshold, the LuxR–AHL complex binds to palindromes within quorum-controlled promoters and activates the expression of QS-dependent genes (1).

Pseudomonas aeruginosa is an opportunistic human pathogen that can cause both acute and chronic infections in hospitalized and immunocompromised hosts. *Pseudomonas aeruginosa* frequently causes life-threatening infections in cystic fibrosis patients; such infections are mediated by multiple QS-regulated virulence factors such as protease, exotoxin, pyocyanin, and biofilms (5–7). Two well-defined AHL QS systems, *las* and *rhl*, exist in *P. aeruginosa* (8). The *las* system consists of the transcriptional regulator LasR and the QS signal synthase LasI. The *lasI* gene product directs the biosynthesis of 3-oxo-C_{12}-HSL, which interacts with LasR and activates target promoters. The *rhl* system consists of the transcriptional activator RhlR and the enzyme RhlI that is responsible for the biosynthesis of C_4-HSL (5,9). In addition to 3-oxo-C_{12}-HSL and C_4-HSL, *P. aeruginosa* produces diverse 2-alkyl-4-quinolones (AHQs) as the third group of QS signal molecules (10). The major AHQ signals include 2-heptyl-3-hydroxy-4-quinolone (the *Pseudomonas* quinolone signal [PQS]) and 2-heptyl-4-quinolone (HHQ) (10,11). PQS synthesis is catalyzed by enzymes encoded by the *pqsABCDE* and *phnAB* operons as well as *pqsH* (11). DNA microarray analysis has revealed that hundreds of genes are controlled by the quorum-sensing systems in *P. aeruginosa* (12).

The *P. aeruginosa* QS circuitry is complex and hierarchical. For example, the post-transcriptional regulator RsmA modulates production of virulence determinants and QS

---

signals by binding to the *lasI* and *rhlI* promoters (13,14); VqsM is a global regulator of QS and virulence factors in *P. aeruginosa* (15). Previously, we have shown that VqsM binds directly to the promoter region of *lasI*, thus controlling QS-regulated phenotypes (16). A number of regulators involved in controlling the activation threshold of quorum-related genes, such as QscR (17,18) and QteE (19), have also been identified. QslA is an anti-activator of QS that regulates virulence factor production by interacting with LasR and preventing it from binding to its target DNA sequence (20,21). Recently, we identified a novel regulator, CdpR, which is required for PQS production and virulence factor expression (22).

Another important regulator, RsaL, acts as a major repressor of the *las* system by binding to the *lasI* promoter, which controls the maximal level of AHLs and thus virulence factor production (23). Microarray results have shown that RsaL regulates at least 341 genes, including the most important virulence genes (i.e. *lasA*, *rhlA* and *phzA1*) (24). As a global regulator, RsaL controls gene expression through different mechanisms including repression of 3-OC_{12}-HSL signal production, direct binding to target genes (such as *phzA1*, *phzM* and *hcnA*), and indirect regulation of several genes via other unknown regulators (25). Moreover, it has been shown that in *P. aeruginosa* $3OC_{12}$-HSL concentration reaches a steady state long before stationary phase (25), indicating that unidentified homeostatic mechanisms contribute to limiting $3OC_{12}$-HSL production. In this study we searched for additional RsaL targets using a ChIP-seq assay. Our results revealed that RsaL binds to the intergenic region between *pqsH* and *cdpR*, which are involved in PQS signal synthesis. Furthermore, our experiments demonstrated that the altered phenotypes of the ∆*rsaL* strain are dependent on PqsH or CdpR expression. Additionally, we report the crystal structure of RsaL bound to DNA, which is reminiscent of a HTH transcription factor bound to dsDNA. In summary, the work presented here identifies RsaL targets involved in QS and provides a molecular structure of RsaL interacting with the promoter region of a QS target.

MATERIALS AND METHODS

Bacterial strains, primers, plasmids and growth conditions

The bacterial strains and plasmids used in this study are listed in Supplementary Table S1. The primers used are detailed in Supplementary Table S2. *P. aeruginosa* PAO1 and derivative strains were grown at 37°C on LB agar plates or in broth with shaking at 220 rpm. Antibiotics were used at the following concentrations: for *Escherichia coli*: 15 µg/ml gentamicin (Gm), 100 µg/ml ampicillin, and 10 µg/ml tetracycline; for *P. aeruginosa*: 50 µg/ml gentamicin (Gm) in LB or 150 µg/ml in PIA (*Pseudomonas* Isolate Agar); 150 µg/ml tetracycline in LB or 300 µg/ml in PIA, and 500 µg/ml carbenicillin in LB.

ChIP-seq analyses

Chromatin immunoprecipitation (ChIP) was performed as previously described (16,26) with minor changes. Wild-type

P. aeruginosa containing empty pAK1900 or pAK1900-RsaL-VSV were cultured in LB medium supplemented with ampicillin until mid-log phase (OD_{600} = 0.6), then treated with 1% formaldehyde for 10 min at 37°C. Cross-linking was stopped by the addition of 125 mM glycine. Bacterial pellets were washed twice with a Tris buffer (20 mM Tris–HCl [pH 7.5] and 150 mM NaCl), re-suspended in 500 µl IP buffer (50 mM HEPES–KOH [pH 7.5], 150 mM NaCl, 1 mM EDTA, 1% Triton X-100, 0.1% sodium deoxycholate, 0.1% SDS, and mini-protease inhibitor cocktail (Roche), and then subjected to sonication to produce 100–300 bp DNA fragments. Insoluble cellular debris was removed by centrifugation at 4°C and the supernatant was used as the input sample in IP experiments. Both control and IP samples were washed with protein A beads (General Electric) and then incubated with 50 µl agarose-conjugated anti-VSV antibodies (Sigma) in IP buffer. Washing, crosslink reversal, and purification of the ChIP DNA were conducted as previously described (26). DNA fragments (150–250 bp) were selected for library construction and sequencing libraries were prepared using the NEXTflex™ ChIP-Seq Kit (Bioo Scientific). The libraries were sequenced using the HiSeq 2000 system (Illumina). ChIP-seq reads were mapped to the *P. aeruginosa* genome, using TopHat (Version 2.0.0) with two mismatches allowed (27). Only uniquely mapped reads were kept for subsequent analyses. The enriched peaks were identified using MACS software (version 2.0.0) (28). The ChIP-seq data files have been deposited in National Center of Biotechnology Information's Gene Expression Omnibus (GEO) and can be accessed through GEO Series accession number GSE87157.

Quantitative PCR

For ChIP-seq peak validation, relative abundance qPCR was performed with Kapa Biosystems Fast Sybr green mix using 16S and 5S rDNA targets as the internal relative standards. Relative target levels were calculated using the $\Delta\Delta C_t$ method with normalization of ChIP targets to the 16S rDNA signal (29).

Expression and purification of the RsaL protein

The full-length *rsaL* gene was amplified by polymerase chain reaction (PCR) from *P. aeruginosa* chromosomal DNA using primers pET-*rsaL*-F/pET-*rsaL*-R (Supplementary Table S2). This PCR product was cloned into pET28a and the resulting plasmid, pET28a-*rsaL*, was transformed into strain BL21 star (DE3). To express the recombinant protein, BL21 strains carrying the pET28a-*rsaL* plasmid were grown in LB medium at 37°C to an OD_{600} of ∼0.6 and the temperature was then reduced to 16°C. Protein expression was induced with 1 mM IPTG (Isopropyl β-D-1-thiogalactopyranoside). And the induced cells were further grown at 16°C for 20 h. To express the seleno-methionine-labeled protein, a 10-ml overnight culture of strain BL21 containing pET28a-*rsaL* was collected and resuspended into 1-l M9 minimal media. The cells were grown at 37°C to an OD_{600} of ∼0.6 and then supplemented with an amino-acid mixture (100 mg lysine (hydrochloride), 100 mg threonine, 100 mg phenylalanine, 50 mg leucine, 50 mg isoleucine,

50 mg valine and 60 mg seleno-methionine). The cells were grown at 37°C for 15 min prior to the addition of 1 mM IPTG and then grown overnight at 37°C before collection.

To purify the recombinant proteins, the cells were resuspended in buffer A (10 mM Tris–HCl [pH 7.5], 500 mM NaCl, 1 mM DTT, and 10 mM PMSF). The cells were lysed by sonication and then centrifuged at 12 000 rpm for 25 min. The supernatant was filtered through a 0.45 μM filter and applied to a Ni-NTA column (Qiagen). The proteins were further purified using a gel-filtration column (Superdex 75, GE Healthcare) with buffer B (10 mM Tris–HCl [pH 7.5], 100 mM NaCl, and 1 mM DTT). Protein purity was verified by SDS-PAGE gel (Supplementary Figure S6A).

Electrophoretic mobility shift assays

Different concentrations of RsaL were incubated with various PCR products (Supplementary Table S2) in 20 μl of gel shift-loading buffer (20 mM Tris–HCl [pH 7.5], 50 mM KCl, 5.0 mM MgCl$_2$, 10% glycerol, and 3 μg/ml sheared salmon sperm DNA). Following incubation at room temperature for 20 min, the samples were analyzed by 6% polyacrylamide gel electrophoresis in 0.5 × TBE (Tris/boric acid/EDTA) buffer at 90 V for 90 min. The gels were stained by SYBR GOLD dye and visualized using a phosphor screen (Tanon 5500).

Plasmid construction

Plasmid *p-rsaL* was constructed by PCR amplifying fragments with the corresponding primer pairs (Supplementary Table S2) p-*rsaL*-F/p-*rsaL*-R. The PCR products were digested with the indicated enzymes and cloned into pAK1900 (30). These same digested PCR products were also cloned into Mini-CTX-lacZ to generate CTX-*rsaL*.

Plasmid pMS402 carrying a promoterless *luxCDABE* reporter gene cluster was used to construct a promoter-*luxCDABE* reporter fusion of the *cdpR* gene, as previously described (31,32). The *cdpR* promoter region was PCR amplified using primers *cdpR-lux*-F (with XhoI site) and *cdpR-lux*-R (with BamHI site) (Supplementary Table S2). The PCR products were cloned into pMS402, yielding pMS402-*cdpR-lux*. In addition, an integration plasmid CTX6.1, originating from plasmid mini-CTX-*lux*, was used to construct a chromosomal fusion reporter; the pMS402 fragment containing a kanamycin-resistance marker, the MCS, and the promoter-*luxCDABE* reporter fusion were isolated and ligated into CTX6.1, yielding CTX-*cdpR-lux*. This plasmid was first transformed into *E. coli* SM10-λ *pir* and the *P. aeruginosa* reporter integration strain was then obtained using biparental mating, as previously reported (33). All constructs were sequenced to verify that no mutations had occurred.

Construction of the *P. aeruginosa* Δ*rsaL* mutant

A SacB-based strategy was employed for the construction of gene knockout mutants, as previously described (22,34). To construct the *rsaL* null mutant (Δ*rsaL*), sequences upstream (1925 bp) and downstream (1866 bp) of the intended deletion were PCR amplified; the upstream fragment was amplified from PAO1 genomic DNA using primer pair pEX-*rsaL*-up-F and pEX-*rsaL*-up-R, while the downstream fragment was amplified with primer pair, pEX-*rsaL*-down-F and pEX-*rsaL*-down-R (Supplementary Table S2). Both PCR products were digested and then cloned into BamHI/HindIII-digested gene replacement vector pEX18Ap, yielding pEX18Ap-*rsaL*. A 0.9 kb gentamicin resistance cassette cut from pPS858 with *Xba*I was then cloned into pEX18Ap-*rsaL*, yielding pEX18Ap-*rsaL*-Gm. The resultant plasmids were electroporated into PAO1 with selection for gentamicin resistance. Colonies were selected for gentamicin resistance and loss of sucrose (5%) susceptibility on LB agar plates containing 50 μg/ml gentamicin and 5% sucrose, which typically indicates a double-cross-over event and thus gene replacement. The Δ*rsaL* mutant was further confirmed by PCR.

Luminescence screening assays

Expression of the *lux*-based reporters in cells grown in liquid culture was measured as counts per second (cps) of light production using a Synergy 2 Plate Reader (Biotek), as previously described (35). Overnight cultures of the reporter strains were diluted to an OD$_{600}$ = 0.2 and cultivated for an additional 2 h prior to use. The cultures were inoculated into parallel wells of a black 96-well plate with a transparent bottom. A 5-μl volume of the fresh cultures was inoculated into the wells containing a total volume of 95 μl medium and the OD$_{600}$ was adjusted to approximately 0.07. A 60-μl volume of filter-sterilized mineral oil was added to prevent evaporation during the assay. Promoter activities were measured every 30 min for 24 h. Bacterial growth was monitored simultaneously by measuring the OD at 595 nm with a Synergy 2 Plate Reader (BioTek).

To determine *lux*-based reporter activity under aerobic conditions, overnight cultures of the reporter strains grown in LB were diluted 1:100 and cultivated in 50 ml plastic tubes. A 100 μl volume of the cultures was transformed every hour into a 96-well black plate and luciferase activity was determined using a Synergy 2 Plate Reader (BioTek).

Biofilm formation assay

Biofilm formation was measured in a static system, as previously described (36), with minor modifications. Visualization of biofilm formation was conducted in 15-ml borosilicate tubes. Briefly, cells from overnight cultures were inoculated at 1:100 dilutions into LB medium supplemented with the appropriate antibiotics and grown at 25°C for 10 h. Biofilms were stained with 0.1% crystal violet (CV) and tubes were washed with water to remove the unbound dye. Quantification of biofilm formation was performed in 24-well polystyrene microtiter plates. Cells were inoculated into LB with appropriate antibiotics to a final OD$_{600}$ of 0.01. The plates were incubated for 8 h or 20 h at 25°C. Crystal violet was added to each tube and stained for 15 min prior to removal by aspiration. Wells were rinsed three times by submerging the tubes in distilled water and the remaining crystal violet was dissolved in 1 ml of 95% ethanol. A 1 ml aliquot of this solution was transferred to a new polystyrene tube and the content was measured at OD$_{600}$.

Measurement of pyocyanin production

Pyocyanin was extracted from culture supernatants and measured as previously described (37). Briefly, 3 ml chloroform was added to 5 ml of culture supernatant. Following extraction, the chloroform layer was transferred to a fresh tube and mixed with 1 ml 0.2 M HCl. Subsequent to centrifugation, the upper layer was removed and its OD_{520} was measured. Concentrations, expressed as μg pyocyanin produced/ml culture supernatant, were determined by multiplying the OD_{520} by 17.072.

Crystallization and data collection

Crystals of the RsaL–DNA complex were grown using the sitting-drop vapor diffusion method at 16°C. The concentrations of RsaL protein and DNA in the crystallization sample were 0.5 and 1.0 mM, respectively. Droplets contained equal volumes of crystallization sample and reservoir solution (0.2 M sodium acetate trihydrate, 0.1 M Tris–HCl [pH 8.5] and 30% polyethylene glycol 4000). Crystals were cryoprotected using their mother liquid supplemented with 20% glycerol and flash-frozen by rapid dipping into liquid nitrogen. The X-ray diffraction data were collected using a beamline BL17U at Shanghai Synchrotron Radiation Facility (SSRF) at cryogenic temperature, maintained with a cryogenic system. The data was collected at a wavelength of 0.97915 Å and processed using the HKL2000 program. Data collection and processing statistics are summarized in Supplementary Table S3.

Structure determination and refinement

The structure of the RsaL–DNA complex was solved using the SAD method (38) with the automatic SHELX C/D/E program embedded in the CCP4i suit (39). The electron density map obtained from the program showed traceable density for the DNA duplex and several α helices, which was manually constructed using the graphics program Coot (40). The partial model was then refined against the diffraction data using the Refmac5 program of CCP4i. During refinement, 5% data was randomly selected and set aside for free R-factor cross validation calculations. The $2F_o - F_c$ and $F_o - F_c$ electron density maps were regularly calculated and used as a guide for the construction of the missing amino acids using Coot. Solvent molecules were also manually built using Coot. The R_{work} and R_{free} of the final structure were 22.3% and 25.6%, respectively; the root mean square deviations (rmsds) of the bond and angle were 0.010° and 1.378°, respectively. The detailed refinement statistics are summarized in Supplementary Table S3. The structure factors and atomic coordinates were deposited in the Protein Data Bank with access code 5J2Y.

RESULTS

Identification of RsaL-binding regions by ChIP-seq

Transcriptomic analysis revealed that RsaL is a global regulator that controls at least 341 genes (24). Several of these targets are QS-controlled genes, whereas others are QS-independent, indicating that RsaL regulates these genes via different mechanisms. To explore the regulatory pathways of RsaL, we performed a ChIP-seq assay to identify additional direct targets of RsaL in the *Pseudomonas* genome. Sequence reads were obtained from two independent ChIP-seq assays using the VSV specific antibody and mapped to the *P. aeruginosa* genome. Using the MACS software, we identified twelve enriched loci harboring RsaL-binding peaks, including the intergenic regions of PA2228/PA2229 and *pqsH*/*cdpR* (Figure 1A), which were enriched by >2.0-fold but were absent in the control samples containing the wild-type *rsaL* gene from PAO1 without the VSV tag. These data were confirmed by quantitative PCR (qPCR) and shown that the enrichment of RsaL ChIP DNA at PA2228 or *pqsH* was higher than the control (Figure 1B).

To verify the enriched *P. aeruginosa* genome loci harboring RsaL-binding peaks, we purified the RsaL protein and performed EMSA on two selected targets, PA2228 and *pqsH*. As shown in Figure 1D, RsaL bound efficiently to both probes in a concentration dependent manner, whereas the negative control *smpB* promoter remained unbound even at the highest concentration (1.0 μM).

RsaL regulates *pqsH* expression and PQS synthesis

Given that RsaL bound to the intergenic region between *pqsH* and *cdpR*, we sought to characterize the specific DNA sequence that RsaL recognizes. To this end, we generated a series of truncated intergenic region fragments (from *pqsH*-P1 to *pqsH*-P8; Supplementary Figure S1A and Supplementary Table S2) and used them to perform EMSAs. RsaL bound to *pqsH*-P1 through *pqsH*-P6 and to *pqsH*-P8, but not to *pqsH*-P7 (Supplementary Figure S1B), suggesting that the binding site is present in *pqsH*-P8. Previous studies have identified a conserved RsaL binding sequence (TATGnAAnTTnCATA) (41). We observed that the sequence (TATTCCATGCGGATG) in the *pqsH*-P8 was similar to the RsaL binding site present in the *lasI* promoter (Figure 2A). Thus, we repeated the EMSA using a truncated *pqsH* probe without this 15-bp motif, which abolished RsaL binding (Figure 2B). In addition, we found similar sequences (TATCGCCCTTGGATG) in the PA2228 promoter region (Supplementary Figure S2A); EMSA showed that RsaL could not bind to the region when this motif was deleted (Supplementary Figure S2B). This result confirmed that the motif is crucial for the DNA-binding ability of RsaL.

Because RsaL binds to the promoter region of *pqsH*, we hypothesized that the expression of *pqsH* is regulated by RsaL. To this end, we generated an *rsaL* deletion strain in the wild-type PAO1 background (ΔrsaL) as well as a ΔrsaL complemented strain (ΔrsaL/CTX-rsaL). Subsequently, the expression of *pqsH* was evaluated in the wild-type PAO1, ΔrsaL strain, and the complemented strain. As shown in Figure 2C, the relative activity of *pqsH* was 3-fold lower in the ΔrsaL strain than in the parental strain. Expression of CTX-rsaL in the *rsaL* mutant could partially restore to wild-type levels. These results clearly suggest that RsaL is a positive regulator of the PQS system.

Biosynthesis of PQS is initiated with the conversion (by the PqsABCD proteins) of anthranilate to HHQ, which is finally converted to PQS by the PqsH monooxygenase. Both HHQ and PQS bind the PqsR regulator and the complex
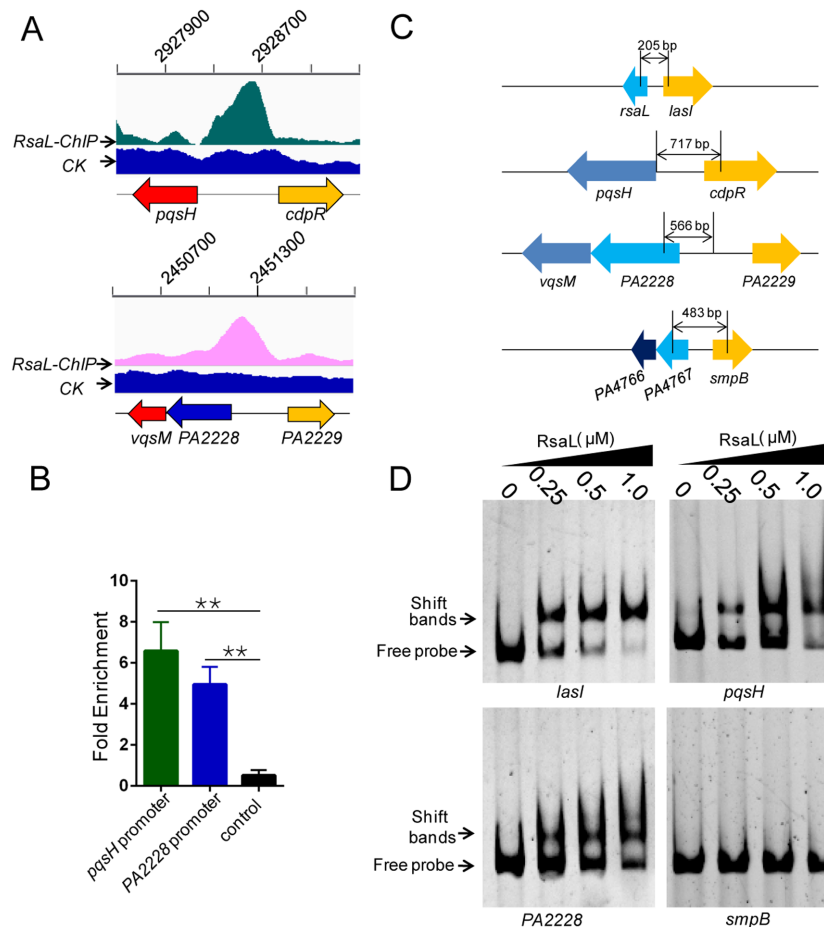
Figure 1. RsaL binds to the intergenic region of *pqsH/cdpR*, and PA2228/PA2229. (**A**) RsaL binding to the identified potential RsaL targets in *P. aeruginosa*, including the intergenic region of *pqsH/cdpR* and PA2228/PA2229. (**B**) RsaL ChIP enrichment of the *pqsH* and PA2228 promoter regions was determined by qPCR relative to sample DNA input. Enrichment of a non-RsaL-dependent promoter (*smpB*) is shown as a control. Significance was determined by a *t* test relative to the *smpB* promoter. **$P < 0.01$. (**C**) Schematic representation of the location of these genes and the fragments for the EMSA experiments. (**D**) EMSAs showing that RsaL binds to the promoter region of *pqsH* and PA2228. PCR products containing *lasI*, *pqsH*, PA2228, and *smpB* promoter regions (as shown in **C**) were added to the reaction mixture at a concentration of 20 ng. The protein concentration for each sample is indicated above its lane. RsaL can efficiently bind to the *lasI* promoter region (positive control); RsaL does not bind to the DNA-probe encompassing P$_{smpB}$ even at a high concentration (negative control).

activates gene expression (11). Because RsaL controls *pqsH* expression, we postulated that it may also influence the expression of the *pqsA* operon and *pqsR*. As predicted, the expression of *pqsR* was drastically decreased in the *rsaL* mutant (Supplementary Figure S3A); however, no effect on *pqsA* expression was observed (Supplementary Figure S3B). Given that PqsH and PqsR are required for PQS synthesis, we next determined PQS levels in the *rsaL* mutant. PQS production was drastically decreased in the *rsaL* mutant compared to wild-type PAO1. Introduction of plasmid p-*rsaL* into the *rsaL* mutant restored PQS production to wild-type levels (Figure 2D); no PQS was detected in the Δ*pqsR* and Δ*pqsH* strains (negative controls). Similarly, we observed that overexpression of *pqsH* in the *rsaL* mutant produced higher levels of PQS than in the wild-type (Figure 2D). Therefore, we conclude that the decrease in PQS production in the *rsaL* mutant was due to inhibition of PQS biosynthesis gene expression during growth.

As previously reported, deletion of *rsaL* leads to the overproduction of secreted virulence factors, including pyocyanin and elastase, and decreases biofilm production (24). Given that RsaL positively regulated *pqsH* expression (Figure 2C), we hypothesized that the altered phenotypes of the *rsaL* mutant were dependent on PqsH activity. Consistent with previous reports, the *rsaL* mutant exhibited enhanced pyocyanin production and reduced biofilm formation (Figure 2E). Strikingly, induction of *pqsH* in the Δ*rsaL* strain appears to complement the biofilm phenotype (Figure 2E and F), probably due to alterations in PQS production. However, expression of *pqsH* in Δ*rsaL* strain was insufficient to return pyocyanin production to wild-type levels (Figure 2E and G), suggesting that the effect of RsaL on pyocyanin is mediated via other pathways.

Deletion of *rsaL* affects the expression of *cdpR*

Given that the ChIP-seq data showed that RsaL binds to the *cdpR* promoter region (the TATTCCATGCGGATG binding sequence is located at −66 to −51 relative to the *cdpR* translational start codon), we hypothesized that RsaL
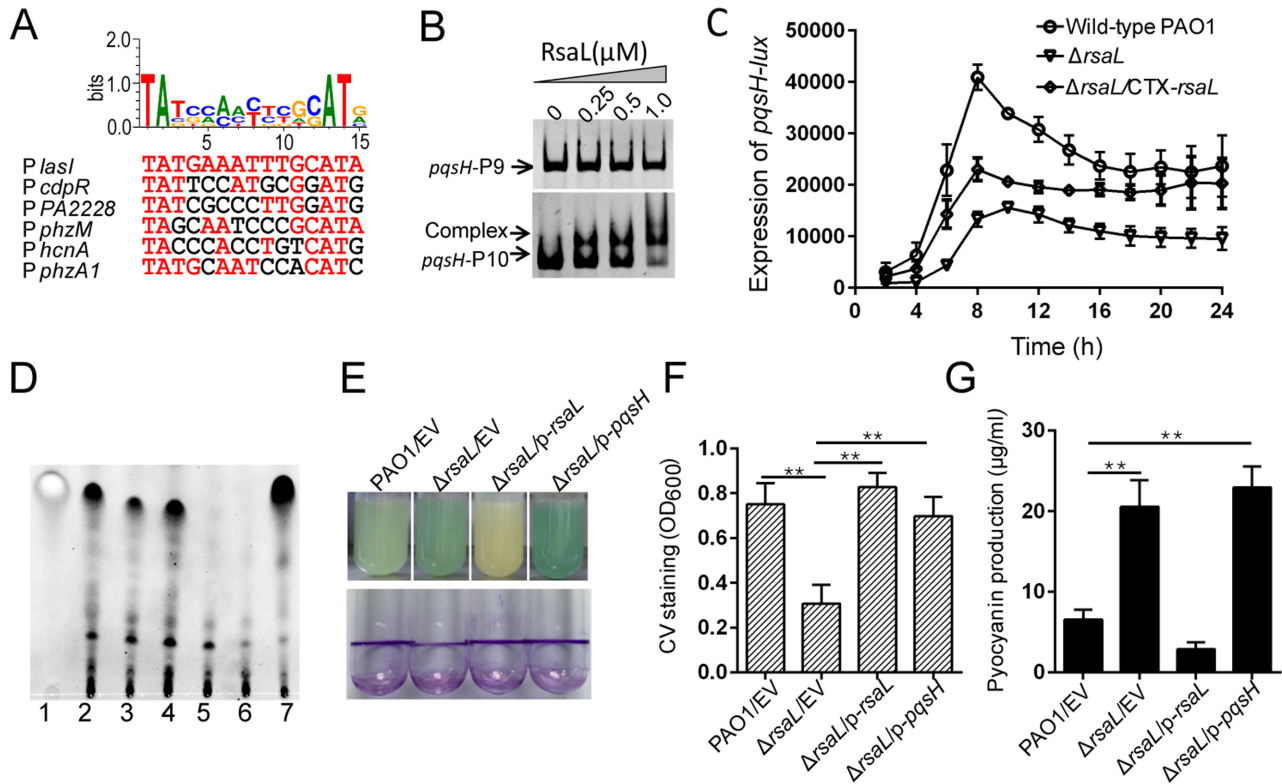
Figure 2. The *rsaL* deletion mutant exhibits reduced *pqsH* activity and PQS production. (**A**) Alignment of the RsaL binding site on P*lasI* with putative RsaL binding sites found in the indicated promoters. Identical residues are highlighted in red. (**B**) Mutation of the binding sites affects the DNA-binding affinity of RsaL. EMSAs show that RsaL cannot bind to the region lacking the binding sites. PCR products containing the *pqsH*-P9 (without the binding sites, see Supplementary Figure S1A) and *pqsH*-P10 regions were added to the reaction mixtures (20 ng). The protein concentration in each sample is indicated above its lane. (**C**) *pqsH-lux* expression was evaluated in the wild-type, *rsaL* mutant, and Δ*rsaL* complemented strain. (**D**) TLC showing that PQS production is lower in the Δ*rsaL* strain than in the wild-type or complemented strains. Expression of *pqsH* in the Δ*rsaL* strain could restore PQS production to wild-type levels. Approximately 400 μl of cultures were subjected to organic extraction and analyzed by TLC. PQS is indicated by the arrowhead. Lane: 1, 25 ng synthetic PQS; 2, wild-type PAO1; 3, *rsaL* mutant; 4, Δ*rsaL* complemented strain; 5, *pqsR* mutant; 6, *pqsH* mutant; 7, Δ*rsaL* strain containing plasmid p-*pqsH*. (**E**) Pyocyanin production (upper row) and biofilm formation (lower row) in the indicated strains. Representative images from at least three independent experiments. (**F, G**) Quantification of biofilm (F) and pyocyanin production (G) in wild-type, *rsaL* mutant, Δ*rsaL* complemented strain and Δ*rsaL* strain containing plasmid p-*pqsH*. Error bars indicate SD from three independent experiments. $^{**}P < 0.01$; t test.

might also modulate the expression of *cdpR*. Therefore, we examined *cdpR* expression in the wild-type, Δ*rsaL* and Δ*rsaL* complemented strains. Remarkably, the relative activity of *cdpR* was reduced approximately 4-fold in the Δ*rsaL* strain compared to the parental strain (Figure 3A). Recently, we reported that CdpR is involved in PQS production by directly regulating *pqsH* expression (22). Similar to the findings for *pqsH*, expression of *cdpR* in the *rsaL* mutant could restore PQS production to wild-type levels (Figure 3B). CdpR is a negative regulator of *P. aeruginosa* virulence factors (22). Therefore, we next investigated whether the altered phenotypes of the *rsaL* mutant are dependent on CdpR. Our results demonstrated that the increased pyocyanin production exhibited by the *rsaL* mutant could be restored to wild-type levels by introducing plasmid p-*cdpR* (Figure 3C and D).

Previously, we reported that CdpR binds to its own promoter region (22). The results of the current study show that RsaL also binds to the intergenic region between *pqsH* and *cdpR*. However, RsaL and CdpR bind two distinct sites on P*cdpR*, suggesting that the two proteins might compete for

binding to this promoter. To test this hypothesis, we performed EMSAs with the DNA encompassing P*cdpR* and purified RsaL and CdpR. As shown in Figure 3E, a supershifted band was observed with both RsaL and CdpR, which did not appear in the presence of RsaL or CdpR alone. This result supports the concept that RsaL and CdpR can bind P*cdpR* simultaneously.

The overall structure of RsaL

To gain additional insights into the interaction between RsaL and its target DNA (TATGAAATTTGCATA, from the *lasI* promoter), we performed structural studies. The complex structure belongs to the $P2_12_12$ space group and the dsDNA duplex forms a complex with an RsaL dimer. The full-length RsaL protein is comprised of 80 amino acids (Figure 4A). However, in the structure, there are six ($_1$MASHER$_6$) and eight ($_1$MASHERTQ$_8$) disordered residues at the N-termini of the two RsaL monomers in the dimer, respectively. The four residues ($_{77}$KIRE$_{80}$) at the C-termini of both RsaL monomers are also disordered. The
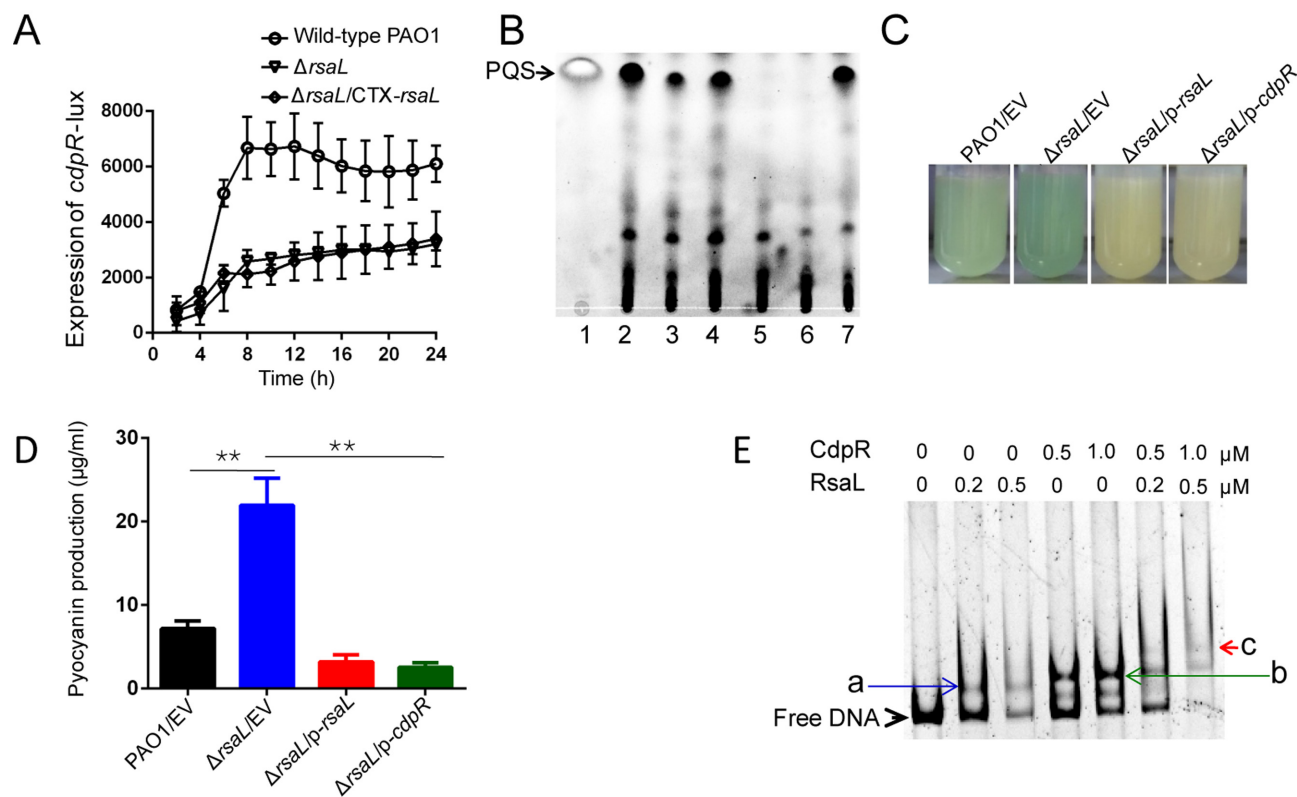
Figure 3. RsaL is required for *cdpR* expression and PQS production. (**A**) The expression of *cdpR* was examined in wild-type PAO1, the *rsaL* mutant, and the Δ*rsaL* complemented strain. Error bars indicate SD from triplicates. (**B**) TLC showing PQS production is lower in the Δ*rsaL* strain than in the wild-type or complemented strains. Expression of *cdpR* in the Δ*rsaL* strain could restore PQS production to wild-type levels. Approximately 400 μl of cultures were subjected to organic extraction and analyzed by TLC. PQS is indicated by arrowhead. Lane: 1, 25 ng synthetic PQS; 2, wild-type PAO1; 3, *rsaL* mutant; 4, Δ*rsaL* complemented strain; 5, *pqsR* mutant; 6, *pqsH* mutant; 7, Δ*rsaL* strain containing plasmid p-*cdpR*. (**C**) Pyocyanin produced by the indicated strains. Representative images from three independent experiments. (**D**) Quantification of pyocyanin production in wild-type, *rsaL* mutant, Δ*rsaL* complemented strain, and Δ*rsaL* strain containing plasmid p-*cdpR*. **$P < 0.01$ compared to wild-type by Student's *t* test. (**E**) EMSA showing that CdpR and RsaL can simultaneously bind to the promoter region of *cdpR*. RsaL and CdpR concentrations are indicated above the lanes. The probe concentration for each sample was 20 ng. Arrows indicate the RsaL/DNA (a, blue), CdpR/DNA (b, green), and RsaL/CdpR/DNA (c, red) complexes.

conformation of both RsaL monomers is quite similar; the root mean square deviations (rmsds) between them are 0.49 Å, based on an alignment of the Ca atoms of residues 7–76. Each RsaL monomer is comprised of five α-helices (α1-α5), which can be divided into two groups: group A and B. Group A contains the first three helices (α1–α3), which assemble as a triangle. Group B is composed of α4 and α5, which form a 'V' shape (Figure 4B). Both α4 and α5 are connected by a three-residue loop ($_{64}$GQI$_{66}$, referred to as the α4-α5 loop) and the angle between the two-helix axis is ∼60°. The group A and group B helices form two layers in the structure, which mainly interact through hydrophobic packing at the N-terminal regions and hydrogen binding at the C-terminal regions of α1 and α4.

RsaL contains several charged residues in its primary amino acid sequence. Of the 80 amino acids of RsaL, 14 residues (including 10 Arg, 2 Lys and 2 His) are positive and 9 residues (7 Glu and 2 Asp) have a negative charge. As shown in Figure 4C, these charged residues form several positive (colored in blue) or negative (colored in red) patches on the surface of the RsaL structure. Interestingly, there is also one hydrophobic patch on the surface of RsaL (Figure 4C, left panel), which may play an im-

portant role in the dimerization of RsaL (Figure 4D). α4 ($_{51}$PFPIYLLLHFYIE$_{63}$) is extremely hydrophobic in nature and sits at the center of the dimer interface (Supplementary Figure S4A). The side chain of Phe60 also interacts hydrophobically with Ile66 of the α4-α5 loop of the partner molecule. Unlike α4, α5 ($_{67}$TDRQLADLRG$_{76}$) is hydrophilic in nature. Of the ten α5 residues, only three (Leu71, Ala712 and Leu74) are hydrophobic; however, interestingly, the side chains of both Leu71 and Leu74 point towards α4 and form hydrophobic interactions with the surrounding residues, including Tyr55, Leu56, His59 and Phe60 (Supplementary Figure S4B). Gln65 is positioned in the middle of the α4-α5 loop and forms two hydrogen bonds (H-bond) with the partner protein: one (2.6 Å) between its NE2 atom and the O atom of Gln65 and the another (3.0 Å) between its OE1 atom and the NE2 atom of Gln70 (Supplementary Figure S4C).

Target DNA recognition by RsaL

In the structure reported in this study, a single RsaL dimer is bound to one target DNA duplex, which is distorted (Figure 5A and Supplementary Figure S5A). Compared with the regular B-form DNA duplex, the width of the minor
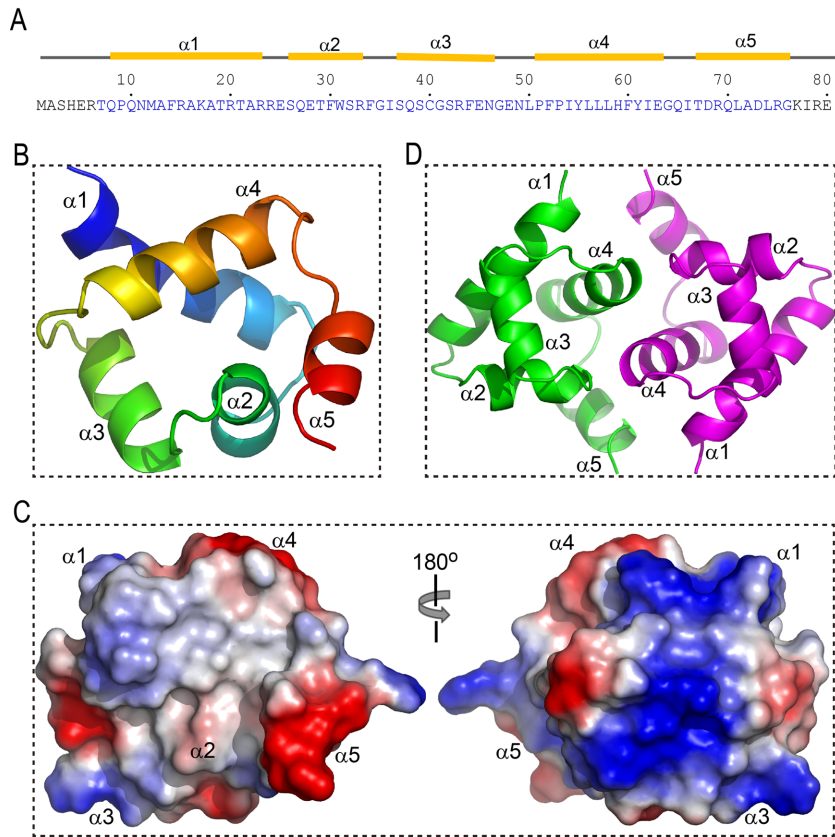
Figure 4. The structure of RsaL. (**A**) The primary sequence and secondary structure of RsaL. The disordered residues in the structure are indicated in gray. (**B**) The overall fold of RsaL. (**C**) Electrostatic representation of RsaL. The positive, negative, and neutrally charged residues are indicated in blue, red and gray, respectively. (**D**) The RsaL dimer observed in the structure.
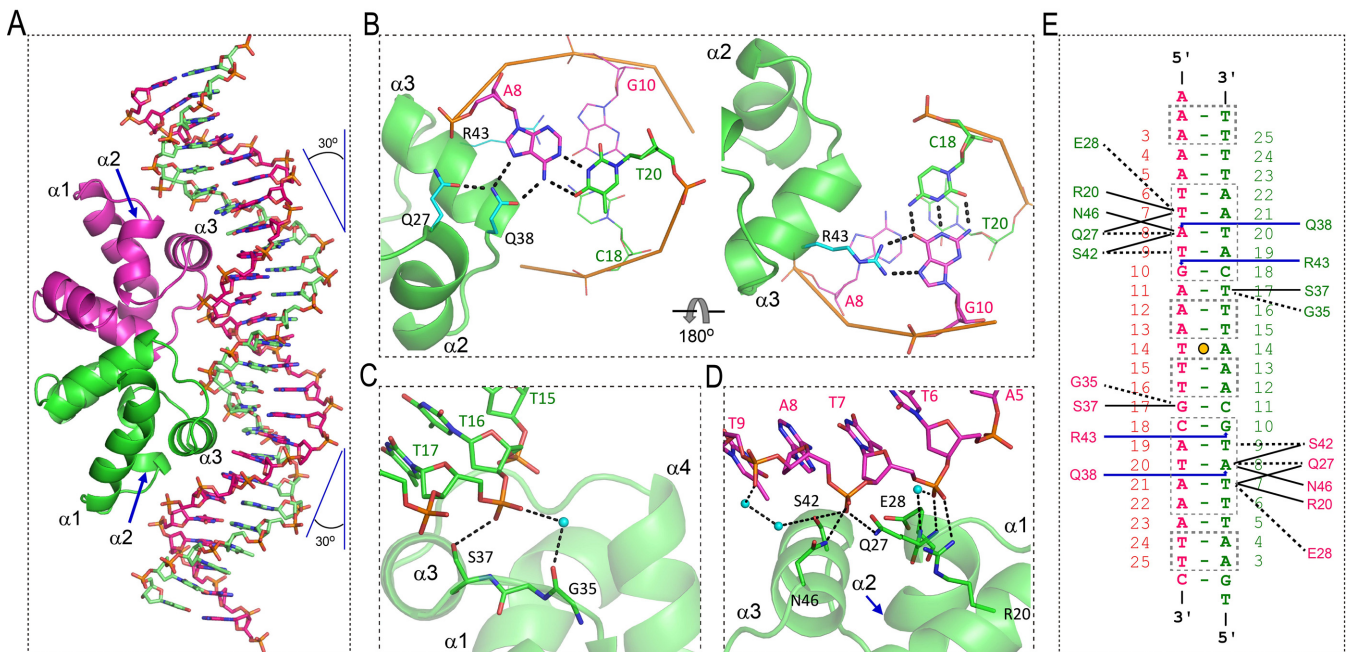
Figure 5. RsaL and target DNA recognition. (**A**) The overall structure of the RsaL–DNA complex. (**B**) DNA base specific recognition by RsaL. (**C**) and (**D**) DNA backbone interaction with RsaL. Cartoon RsaL molecules are shown in purple and green, respectively. The DNA and protein residues involved in DNA binding are depicted as sticks. (**E**) Schematic presentation illustrating the DNA–protein interactions observed in the structure.

groove at the central segment (including base pairs T12:A16 to T16:A12) of the target DNA is ~3 Å shorter; it was also narrowed by 2–3 Å at two other regions: region A (including base pairs A4:T24 to T7:A21) and region B (including base pairs A21:T7 to T24:A4). The other segment of the target DNA adopts a conformation similar to the regular B-form DNA duplex; however, in contrast to the extended conformation of the B-form DNA duplex, the helical axis of the target DNA was bent at 30° toward the RsaL molecules at both ends (Figure 5A).

RsaL interacts with the target DNA mainly via the group A helices, especially α3 ($_{37}$SQSCGSRFEN$_{46}$), which packs against the DNA major groove. The side chains of two residues (Gln38 and Arg43) of α3 form sequence-specific interactions with the target DNA. Gln38 is located at the N-terminus of α3 and forms two H-bonds with the A8 nucleotide of the A8:T20 base pair (Figure 5B, left panel): one H-bond (2.6 Å) is between its OE1 and the N6 atom of A8 and the other (2.6 Å) is between its NE2 atom and the N7 atom of A8. Gln38 also forms one H-bond (2.8 Å) with the side chain of Gln27, which may further stabilize the conformation of Gln38. Arg43 resides in the middle of α3 and can recognize the G10:C18 base pair. Arg43 forms two H-bonds with G10: one (3.0 Å) between its NH1 atom and the O6 atom of G10 and the other (3.0 Å) between its NH2 atom and the N7 atom of G10 (Figure 5B, right panel).

In addition to the base pairs, RsaL also interacts with the backbone of the target DNA via residues within the group A helices. The residues of α3 are also involved in these interactions. Ser37 is the first residue of α3 and its OG atom forms one H-bond (3.0 Å) with the OP2 atom of nucleotide T17, which in turn interacts with Gly35 via water-mediated H-bonds (Figure 5C). Another two residues of α3, Ser42 and Asn46 (which reside in the middle and at the C-terminus, respectively), also interact with the DNA backbone. As depicted in Figure 5D, the side chains of Ser42 and Asn46 form H-bonds with the phosphate group of the same nucleotide, A8. The distance between the ND2 atom of Asn46 and the OP1 atom of A8 is 3.1 Å. The interaction between Ser42 and A8 is stronger, indicated by the short distance (2.6 Å) between the OG atom of Ser42 and the OP2 atom of A8. Similar to Ser37, Ser42 can also interact with the DNA backbone (the OP2 atom of T9) via water mediated H-bonds.

Three residues from helices α1 and α2 also participate in DNA backbone recognition (Figure 5D). Arg20 of α1 interacts with the DNA via both a direct H-bond (the distance between the NH1 atom of Arg20 and the OP1 atom of T7 is ~2.8 Å) and an indirect water-mediated H-bond. Gln27 and Glu28 are the second and the third residues of α2, respectively. Gln27 interacts with DNA via two H-bonds: one (2.9 Å) between its backbone N atom and the OP2 atom of T7 and the other (2.9 Å) between its NE2 atom and the OP2 atom of A8. Glu28 also interacts with DNA (the OP1 atom of T7); however, unlike Gln27, the interaction between Glu28 and T7 is mediated by a water molecule.

The target DNA duplex is comprised of two single strand DNA sequences (Figure 5E), DNA_F: 5′-AAAAATTATGAAATTTGCATAAATTC-3′ and DNA_R: 5′- TGAATTTATGCAAATTTCATAATTTT-3′. Except for the two nucleotides at the 5′-end and one

nucleotide at the 3′-end, the sequences of DNA_F and DNA_R are actually quite similar, as highlighted by the underline. In the structure, the DNA duplex and the RsaL dimer are related by a two-fold axis located at the middle of the T14:A14 pairs (Supplementary Figure S5); the RsaL–DNA interactions described above are also conserved for the other RsaL molecule. The sequence of the DNA duplex is palindromic, which parallels the dimeric conformation of RsaL.

Validation of the key functional residues in RsaL

The crystal structure of the RsaL–DNA complex provides insight into the protein-DNA interactions (Figure 5 and Supplementary Figure S5). We next sought to experimentally confirm the function of a number of conserved residues in RsaL *in vivo* and *in vitro*. To this end, the residues predicted to contact DNA (Gln38, Gln27, Glu28, and Arg43) and form the salt bridge (Arg20 and Glu45) were mutated to Ala. Given that RsaL can efficiently bind to the *lasI* promoter region, we compared the binding abilities of the wild-type and mutated variants of RsaL *in vitro* by EMSA. The mutated proteins were expressed and purified; SDS-PAGE showed that all mutated derivatives of RsaL, except for R20A, were expressed at the same level as wild-type RsaL (Supplementary Figure S6A). The oligomeric state of the RsaL mutants was examined by analytical size exclusion chromatography; all mutants exhibited dimerization (Supplementary Figure S6B). The EMSA data revealed that RsaL^{wt} was able to shift nearly 100% of the *lasI* probe at a concentration of 25 nM, whereas RsaL^{Q38A}, RsaL^{R43A}, RsaL^{Q27A}, RsaL^{G35A}, RsaL^{S37A} and RsaL^{S42A}, were unable to shift the same DNA probe even at a concentration of 1.0 μM (Figure 6A). Taken together, the EMSA results confirm that Arg20, Arg43, Gln27, Gln38, Gly35, Ser37, and Ser42, are important for establishing direct interactions between RsaL and DNA, which is consistent with our structural model.

The expression of *lasI* has been shown to increase in an *rsaL* mutant of *P. aeruginosa* PAO1 (23). Thus, we used this phenotype to compare the *in vivo* activity of the wild-type and mutated variants of RsaL using a complementation assay. The wild-type and mutated coding sequences of *rsaL* were cloned into plasmid pAK1900 and independently introduced into the Δ*rsaL* strain which contained the *lasI* promoter fusion CTX-*lasI-lux*. The results of this experiment showed that the expression of *lasI* was enhanced approximately 5-fold in the *rsaL* mutant compared with the parental strain (Figure 6B). Complementation of this mutant with *rsaL* or its mutated variants *rsaL*^{E28A} and *rsaL*^{N46A} restored the activity of *lasI* to wild-type levels. Conversely, the transcriptional level of *lasI* was not complemented by introducing plasmids containing *rsaL*^{R20A}, *rsaL*^{R43A}, *rsaL*^{Q38A}, *rsaL*^{Q27A}, *rsaL*^{G35A}, *rsaL*^{S37A} or *rsaL*^{S42A} (Figure 6B). Combined with the *in vitro* results, these results clearly demonstrate that RsaL residues Arg20, Arg43, Gln27, Gln38, Gly35, Ser37 and Ser42 are essential for RsaL activity in the cell.
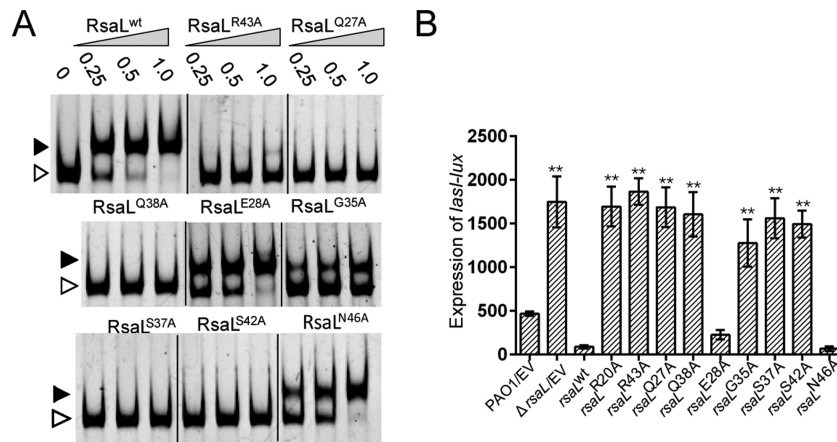
Figure 6. EMSA and promoter activity experiments indicating that certain residues of RsaL are important for RsaL–DNA interaction. (**A**) EMSA carried out with a DNA probe (P*lasI*) and either RsaL[wt] or its mutated derivatives (indicated above each gel). The protein concentration for each sample is indicated above its lane. Free-DNA is indicated by a non-filled triangle and the RsaL–DNA complexes are indicated by filled triangles. (**B**) The Effects of wild-type RsaL and its mutants on *lasI* promoter fusion expression *in vivo*. The Δ*rsaL* strain carrying a *lasI-lux* reporter was transformed with either an empty vector (EV), wild-type *rsaL*, or its mutated derivatives, as indicated. Error bars indicate SD from three independent experiments. [**]*P* < 0.01 compared to wild-type by Student's *t* test.

DISCUSSION

The QS systems of *P. aeruginosa* consist of complex regulatory networks and play an important role in the pathogenicity of this bacterium. However, the detailed regulatory mechanisms of a number of QS regulators remain elusive. Previous studies have shown that RsaL is a repressor of the *las* system (23,25); however, it remains uncharacterized otherwise. Here, we performed ChIP-seq and EMSA experiments that identified two new *in vivo* binding sites of RsaL in the *P. aeruginosa* genome. We also solved the crystal structure of the RsaL–DNA complex. The combination of the present ChIP-seq results and structural model of RsaL should provide a much better understanding of the regulatory mechanisms of RsaL.

Of the two RsaL-bound regions, one is located in the PA2225-PA2228 operon and the other is the intergenic region between *pqsH* and PA2588. However, other targets identified from ChIP-seq assays are not bound by RsaL using EMSA. In addition, some previously established direct targets (such as *lasI*, *phzA1*, *phzM* and *hcnA*) were not identified in the present work. The omission of these genes may be due to the conditions used in the present study (i.e. using the pAK1900 vector and mid-log phase cultures), thus, further optimization of this method is needed. Importantly, the ChIP-seq data and EMSA analysis showed that RsaL binds efficiently to the intergenic region between *pqsH* and *cdpR* (Figure 1), which explains the reduction in *pqsH*/*cdpR* transcription level and PQS production in the *rsaL* mutant (Figures 2 and 3). Previous microarray results have shown that RsaL can control several hundreds of genes, including the most important virulence genes involved in biofilm formation and pyocyanin production (24,25). Based on these observations, RsaL most probably enables the control of QS-regulated phenotypes via PqsH or CdpR. In agreement with this hypothesis, expression of *pqsH* in the *rsaL* mutant was sufficient to restore wild-type biofilm production levels (Figure 2E and F). Moreover, RsaL is required for *cdpR* expression and the altered pyocyanin production in

the Δ*rsaL* strain is dependent on CdpR (Figure 3). Therefore, RsaL can control these virulence genes via multiple pathways including direct binding to their promoters and indirectly blocking *las* or *pqs*-dependent transcription.

To further elucidate the QS regulatory networks, the crystal structures of two QS-related proteins have been solved; the Bottomley *et al.* reported the crystal structure of the LasR ligand-binding domain bound to its autoinducer 3-oxo-C_{12}-acylhomoserine lactone (42) and the Lintz *et al* determined the structure of the QS repressor QscR bound to N-3-oxo-dodecanoyl-homoserine lactone (18). A BLASTP search of the RsaL amino acid sequence did not reveal significant homology with functionally characterized proteins in *P. aeruginosa*. Therefore, we determined the crystal structure of the RsaL–DNA complex. RsaL mainly interacts with the target DNA using its α3 helix ($_{37}$SQSCGSRFEN$_{46}$), which packs against the DNA major groove and recognizes the base pairs (Figure 5). Furthermore, one residue (Arg20) from α1 and two residues (Gln27 and Glu28) from α2 also participate in DNA backbone recognition (Figure 5D). RsaL has no significant sequence similarity to any known proteins in other species; however, the DALI server program (43) revealed that the overall fold of RsaL is similar to the HTH domains (Supplementary Figure S7A) conserved in many DNA transcriptional regulators, such as HNF6 (44), SATB1 (45), MqsA (46) and Oct1 (47). Although obvious differences can be observed in the α1 and α5 regions, the conformations of the three central helixes (α2–α4) of RsaL are quite similar to these HTH domain structures (Supplementary Figure S7A). Similar to RsaL, MqsA interacts with DNA as a dimer (Supplementary Figure S7B). Oct1 and HNF6 function as monomers and in addition to their primary HTH domains, their additional HTH domains (HTH2) are also involved in target DNA recognition (Supplementary Figure S7C). The relative orientations of the HTH2 domains in the Oct1 and HNF6 structures are different from one another; however, the orientations of the HTH domains
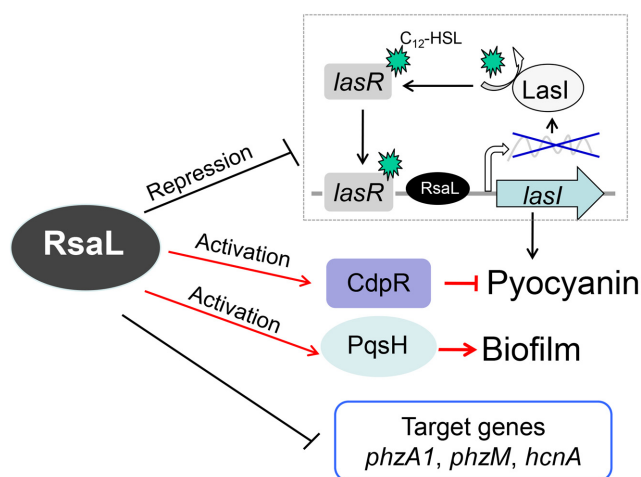
Figure 7. Schematic model of RsaL involved in the QS regulatory cascade and virulence factor regulation of *P. aeruginosa*. The potential regulatory pathways and interplays of RsaL are based on our observations and those of previous studies. It has been demonstrated that RsaL, in concert with LasR, govern the homeostasis of $3OC_{12}$-HSL by controlling the expression of *rsaL* and *lasI* (25). In the present study, we show that RsaL binds directly to the intergenic region of *pqsH/cdpR*, thus controlling PQS production and *P. aeruginosa* virulence phenotypes. Solid arrows indicate positive regulation and solid T-bars represent negative regulation.

and their interactions with the target DNAs are conserved among all of the structures. Structure based sequence alignment showed that most of the DNA recognition residues are also conserved in these structures (Supplementary Figure S7D); the conservation of the residues and their interactions with DNA bases suggest that other HTH domain-containing proteins may also use the same strategy in target DNA recognition.

In summary, our findings extend understanding of the functions of the QS repressor RsaL. In addition to being involved in regulating the $3OC_{12}$-HSL, RsaL also controls the activity of *pqsH* and *cdpR*, which are both required for PQS synthesis. Therefore, cross-regulation between *lasI* and *pqsH/cdpR* in the *rsaL* mutant maintains a balanced level of signal production in *P. aeruginosa*. Importantly, the major function of RsaL in *P. aeruginosa* physiology is to govern the homeostasis of $3OC_{12}$-HSL by controlling, together with LasR, the expression of *rsaL* and *lasI* (25). Moreover, RsaL is a global regulator that is an integral part of the QS signaling network, which controls gene expression through different mechanisms, including repression of $3OC_{12}$-HSL signal molecule production, activation of PQS synthesis, and direct binding of target genes (Figure 7). Therefore, the broad range of RsaL functions further elucidates the complexity of the QS network and the detailed characterization of the RsaL–DNA complex will provide new clues for understanding other QS regulators.

SUPPLEMENTARY DATA

Supplementary Data are available at NAR Online.

REFERENCES

1. Fuqua,W.C., Winans,S.C. and Greenberg,E.P. (1994) Quorum sensing in bacteria: the LuxR-LuxI family of cell density-responsive transcriptional regulators. *J. Bacteriol.*, **176**, 269–275.
2. Waters,C.M. and Bassler,B.L. (2005) Quorum sensing: cell-to-cell communication in bacteria. *Annu. Rev. Cell Dev. Biol.*, **21**, 319–346.
3. Bassler,B.L. (2002) Small talk. Cell-to-cell communication in bacteria. *Cell*, **109**, 421–424.
4. Fuqua,C. and Greenberg,E.P. (2002) Listening in on bacteria: acyl-homoserine lactone signalling. *Nat. Rev. Mol. Cell Biol.*, **3**, 685–695.
5. Smith,R.S. and Iglewski,B.H. (2003) *P.aeruginosa* quorum-sensing systems and virulence. *Curr. Opin. Microbiol.*, **6**, 56–60.
6. Davies,D.G., Parsek,M.R., Pearson,J.P., Iglewski,B.H., Costerton,J.W. and Greenberg,E.P. (1998) The involvement of cell-to-cell signals in the development of a bacterial biofilm. *Science*, **280**, 295–298.
7. Gambello,M.J., Kaye,S. and Iglewski,B.H. (1993) LasR of *Pseudomonas aeruginosa* is a transcriptional activator of the alkaline protease gene (apr) and an enhancer of exotoxin A expression. *Infect. Immun.*, **61**, 1180–1184.
8. Pearson,J.P., Passador,L., Iglewski,B.H. and Greenberg,E.P. (1995) A second N-acylhomoserine lactone signal produced by *Pseudomonas aeruginosa*. *Proc. Natl. Acad. Sci. U.S.A.*, **92**, 1490–1494.
9. Fuqua,C., Winans,S.C. and Greenberg,E.P. (1996) Census and consensus in bacterial ecosystems: the LuxR-LuxI family of quorum-sensing transcriptional regulators. *Annu. Rev. Microbiol.*, **50**, 727–751.
10. Pesci,E.C., Milbank,J.B., Pearson,J.P., McKnight,S., Kende,A.S., Greenberg,E.P. and Iglewski,B.H. (1999) Quinolone signaling in the cell-to-cell communication system of *Pseudomonas aeruginosa*. *Proc. Natl. Acad. Sci. U.S.A.*, **96**, 11229–11234.
11. Deziel,E., Lepine,F., Milot,S., He,J., Mindrinos,M.N., Tompkins,R.G. and Rahme,L.G. (2004) Analysis of *Pseudomonas aeruginosa* 4-hydroxy-2-alkylquinolines (HAQs) reveals a role for 4-hydroxy-2-heptylquinoline in cell-to-cell communication. *Proc. Natl. Acad. Sci. U.S.A.*, **101**, 1339–1344.
12. Schuster,M., Lostroh,C.P., Ogi,T. and Greenberg,E.P. (2003) Identification, timing, and signal specificity of *Pseudomonas aeruginosa* quorum-controlled genes: a transcriptome analysis. *J. Bacteriol.*, **185**, 2066–2079.
13. Pessi,G., Williams,F., Hindle,Z., Heurlier,K., Holden,M.T., Camara,M., Haas,D. and Williams,P. (2001) The global posttranscriptional regulator RsmA modulates production of virulence determinants and N-acylhomoserine lactones in *Pseudomonas aeruginosa*. *J. Bacteriol.*, **183**, 6676–6683.
14. Kay,E., Humair,B., Denervaud,V., Riedel,K., Spahr,S., Eberl,L., Valverde,C. and Haas,D. (2006) Two GacA-dependent small RNAs modulate the quorum-sensing response in *Pseudomonas aeruginosa*. *J. Bacteriol.*, **188**, 6026–6033.
15. Dong,Y.H., Zhang,X.F., Xu,J.L., Tan,A.T. and Zhang,L.H. (2005) VqsM, a novel AraC-type global regulator of quorum-sensing signalling and virulence in *Pseudomonas aeruginosa*. *Mol. Microbiol.*, **58**, 552–564.
16. Liang,H., Deng,X., Li,X., Ye,Y. and Wu,M. (2014) Molecular mechanisms of master regulator VqsM mediating quorum-sensing and antibiotic resistance in *Pseudomonas aeruginosa*. *Nucleic Acids Res.*, **42**, 10307–10320.

17. Chugani,S.A., Whiteley,M., Lee,K.M., D'Argenio,D., Manoil,C. and Greenberg,E.P. (2001) QscR, a modulator of quorum-sensing signal synthesis and virulence in *Pseudomonas aeruginosa*. *Proc. Natl. Acad. Sci. U.S.A.*, **98**, 2752–2757.

18. Lintz,M.J., Oinuma,K., Wysoczynski,C.L., Greenberg,E.P. and Churchill,M.E. (2011) Crystal structure of QscR, a *Pseudomonas aeruginosa* quorum sensing signal receptor. *Proc. Natl. Acad. Sci. U.S.A.*, **108**, 15763–15768.

19. Siehnel,R., Traxler,B., An,D.D., Parsek,M.R., Schaefer,A.L. and Singh,P.K. (2010) A unique regulator controls the activation threshold of quorum-regulated genes in *Pseudomonas aeruginosa*. *Proc. Natl. Acad. Sci. U.S.A.*, **107**, 7916–7921.

20. Seet,Q. and Zhang,L.H. (2011) Anti-activator QslA defines the quorum sensing threshold and response in *Pseudomonas aeruginosa*. *Mol. Microbiol.*, **80**, 951–965.

21. Fan,H., Dong,Y., Wu,D., Bowler,M.W., Zhang,L. and Song,H. (2013) QsIA disrupts LasR dimerization in antiactivation of bacterial quorum sensing. *Proc. Natl. Acad. Sci. U.S.A.*, **110**, 20765–20770.

22. Zhao,J., Yu,X., Zhu,M., Kang,H., Ma,J., Wu,M., Gan,J., Deng,X. and Liang,H. (2016) Structural and molecular mechanism of CdpR involved in quorum-sensing and bacterial virulence in *Pseudomonas aeruginosa*. *PLoS Biol.*, **14**, e1002449.

23. Rampioni,G., Bertani,I., Zennaro,E., Polticelli,F., Venturi,V. and Leoni,L. (2006) The quorum-sensing negative regulator RsaL of *Pseudomonas aeruginosa* binds to the lasI promoter. *J. Bacteriol.*, **188**, 815–819.

24. Rampioni,G., Schuster,M., Greenberg,E.P., Zennaro,E. and Leoni,L. (2009) Contribution of the RsaL global regulator to *Pseudomonas aeruginosa* virulence and biofilm formation. *FEMS Microbiol. Lett.*, **301**, 210–217.

25. Rampioni,G., Schuster,M., Greenberg,E.P., Bertani,I., Grasso,M., Venturi,V., Zennaro,E. and Leoni,L. (2007) RsaL provides quorum sensing homeostasis and functions as a global regulator of gene expression in *Pseudomonas aeruginosa*. *Mol. Microbiol.*, **66**, 1557–1565.

26. Blasco,B., Chen,J.M., Hartkoorn,R., Sala,C., Uplekar,S., Rougemont,J., Pojer,F. and Cole,S.T. (2012) Virulence regulator EspR of *Mycobacterium tuberculosis* is a nucleoid-associated protein. *PLoS Pathog.*, **8**, e1002621.

27. Trapnell,C., Pachter,L. and Salzberg,S.L. (2009) TopHat: discovering splice junctions with RNA-Seq. *Bioinformatics*, **25**, 1105–1111.

28. Zhang,Y., Liu,T., Meyer,C.A., Eeckhoute,J., Johnson,D.S., Bernstein,B.E., Nusbaum,C., Myers,R.M., Brown,M., Li,W. *et al.* (2008) Model-based analysis of ChIP-Seq (MACS). *Genome Biol.*, **9**, R137.

29. Livak,K.J. and Schmittgen,T.D. (2001) Analysis of relative gene expression data using real-time quantitative PCR and the 2(-Delta Delta C(T)) Method. *Methods*, **25**, 402–408.

30. Poole,K., Neshat,S., Krebes,K. and Heinrichs,D.E. (1993) Cloning and nucleotide sequence analysis of the ferripyoverdine receptor gene *fpvA* of *Pseudomonas aeruginosa*. *J. Bacteriol.*, **175**, 4597–4604.

31. Liang,H., Duan,J., Sibley,C.D., Surette,M.G. and Duan,K. (2011) Identification of mutants with altered phenazine production in *Pseudomonas aeruginosa*. *J. Med. Microbiol.*, **60**, 22–34.

32. Duan,K., Dammel,C., Stein,J., Rabin,H. and Surette,M.G. (2003) Modulation of *Pseudomonas aeruginosa* gene expression by host microflora through interspecies communication. *Mol. Microbiol.*, **50**, 1477–1491.

33. Hoang,T.T., Kutchma,A.J., Becher,A. and Schweizer,H.P. (2000) Integration-proficient plasmids for *Pseudomonas aeruginosa*: site-specific integration and use for engineering of reporter and expression strains. *Plasmid*, **43**, 59–72.

34. Hoang,T.T., Karkhoff-Schweizer,R.R., Kutchma,A.J. and Schweizer,H.P. (1998) A broad-host-range Flp-FRT recombination system for site-specific excision of chromosomally-located DNA sequences: application for isolation of unmarked *Pseudomonas aeruginosa* mutants. *Gene*, **212**, 77–86.

35. Liang,H., Li,L., Dong,Z., Surette,M.G. and Duan,K. (2008) The YebC family protein PA0964 negatively regulates the *Pseudomonas aeruginosa* quinolone signal system and pyocyanin production. *J. Bacteriol.*, **190**, 6217–6227.

36. O'Toole,G.A. and Kolter,R. (1998) Flagellar and twitching motility are necessary for *Pseudomonas aeruginosa* biofilm development. *Mol. Microbiol.*, **30**, 295–304.

37. M,K. (1958) Studies on the biosynthesis of pyocyanine. Isolation and determination of pyocyanine. *Bull. Inst. Chem. Res. Kyoto Univ.*, **36**, 163–173.

38. Giacovazzo,C. and Siliqi,D. (2004) Phasing via SAD/MAD data: the method of the joint probability distribution functions. *Acta Crystallogr. D Biol. Crystallogr.*, **60**, 73–82.

39. Potterton,E., Briggs,P., Turkenburg,M. and Dodson,E. (2003) A graphical user interface to the CCP4 program suite. *Acta Crystallogr. D Biol. Crystallogr.*, **59**, 1131–1137.

40. Emsley,P. and Cowtan,K. (2004) Coot: model-building tools for molecular graphics. *Acta Crystallogr. D Biol. Crystallogr.*, **60**, 2126–2132.

41. Rampioni,G., Polticelli,F., Bertani,I., Righetti,K., Venturi,V., Zennaro,E. and Leoni,L. (2007) The *Pseudomonas* quorum-sensing regulator RsaL belongs to the tetrahelical superclass of H-T-H proteins. *J. Bacteriol.*, **189**, 1922–1930.

42. Bottomley,M.J., Muraglia,E., Bazzo,R. and Carfi,A. (2007) Molecular insights into quorum sensing in the human pathogen *Pseudomonas aeruginosa* from the structure of the virulence regulator LasR bound to its autoinducer. *J. Biol. Chem.*, **282**, 13592–13600.

43. Holm,L. and Rosenstrom,P. (2010) Dali server: conservation mapping in 3D. *Nucleic Acids Res.*, **38**, W545–W549.

44. Iyaguchi,D., Yao,M., Watanabe,N., Nishihira,J. and Tanaka,I. (2007) DNA recognition mechanism of the ONECUT homeodomain of transcription factor HNF-6. *Structure*, **15**, 75–83.

45. Yamasaki,K., Akiba,T., Yamasaki,T. and Harata,K. (2007) Structural basis for recognition of the matrix attachment region of DNA by transcription factor SATB1. *Nucleic Acids Res.*, **35**, 5073–5084.

46. Brown,B.L., Wood,T.K., Peti,W. and Page,R. (2011) Structure of the *Escherichia coli* antitoxin MqsA (YgiT/b3021) bound to its gene promoter reveals extensive domain rearrangements and the specificity of transcriptional regulation. *J. Biol. Chem.*, **286**, 2285–2296.

47. Klemm,J.D. and Pabo,C.O. (1996) Oct-1 POU domain-DNA interactions: cooperative binding of isolated subdomains and effects of covalent linkage. *Genes Dev.*, **10**, 27–36.